Sensors and Actuators: A. Physical 333 (2022) 113255

Contents lists available at ScienceDirect

Sensors and Actuators: A. Physical

journal homepage: www.elsevier.com/locate/sna

# The effect of morphology on poly(vinylidene fluoride-trifluoroethylene-chlorotrifluoroethylene)-based soft actuators: Films and electrospun aligned nanofiber mats

Riccardo D'Anniballe[a,*,1], Andrea Zucchelli[b,2], Raffaella Carloni[a,3]

[a] Bernoulli Institute for Mathematics, Computer Science and Artificial Intelligence, Faculty of Science and Engineering, University of Groningen, Nijenborgh 9, 9747AG Groningen, The Netherlands

[b] Interdepartmental Centre for Industrial Research in Advanced Mechanical Engineering Applications and Materials Technology, Department of Industrial Engineering, University of Bologna, Viale Risorgimento 2, 40136 Bologna, Italy

ARTICLE INFO

*Article history:*
Received 30 September 2021
Received in revised form 23 November 2021
Accepted 28 November 2021
Available online 1 December 2021

*Keywords:*
P(VDF-TrFE-CTFE)
Nanofibers
Electrostriction
Soft actuators

ABSTRACT

This paper analyzes soft actuators realized as unimorph cantilever beams, in which the active layer can have two different morphologies, i.e., either an extruded film or an aligned electrospun nanofiber mat of the poly (vinylidene fluoride-trifluoroethylene-chlorotrifluoroethylene). Six different soft actuators are fabricated, with active layers of varying thicknesses and morphologies, to study the electrostrictive effect of the polymer and to evaluate the stiffening properties, the mechanical work, and the blocking forces of the actuators when stimulated by different direct current electric fields. The comparison between the different actuators is performed by introducing weight specific properties, i.e., specific stiffness and specific work, showing improved specific properties for the nanofibers-based actuators. Moreover, the blocking forces, the tip deflections, and the leakage currents of the actuators are evaluated when stimulated by alternating current electric fields. The experiments show faster viscoelastic relaxation and lower electrical power consumption for the nanofibers-based actuators. This study concludes that, thank to its electro-mechanical properties, the poly(vinylidene fluoride-trifluoroethylene-chlorotrifluoroethylene) in the form of aligned electrospun nanofiber mat has high potential to be used as the active layer of electrostrictive unimorph beam soft actuators.



## 1. Introduction

The poly(vinylidene fluoride-trifluoroethylene-chlorotrifluoroethylene) (P(VDF-TrFE-CTFE)) is a relaxor ferroelectric polymer that shows a high electrostrictive strain, i.e., the ability to produce a large field-induced strain when exposed to an external electric field [1,2]. In the pursuit of designing soft bending actuators with a stiffening behavior, this study analyzes different P(VDF-TrFE-CTFE)-based soft actuators, which have been designed as layered unimorph cantilever beams. Specifically, the active layer is either a film of P(VDF-TrFE-CTFE) or a mat of P (VDF-TrFE-CTFE) aligned nanofibers that have been realized by electrospinning, a nano/micro fabrication process that can stretch a polymeric solution through a high electrostatic field [3].

In the literature, the effect of changes in the morphology of PVDF-based soft actuators, processed either in thin extruded/cast films or electrospun random/aligned nanofiber mats, has been analyzed. Table 1 summarizes the main contributions to the state of the art with respect to the configuration of the actuators, used active material, evaluated actuation properties, and the general advantages given by the nanofibrous morphology, when an explicit comparison on the actuation properties with respect to the film is performed. In [4], cantilever beam actuators made of electrospun nanofibers of PVDF and carbon nanotubes (CNT) exhibit larger displacements, enhanced electrical conductivity, and interfacial properties compared to a cast PVDF-based actuator. In [5], an electrospun poly(vinylidene fluoride-co-hexafluoropropylene) (P(VDF-HFP)) mat shows improved electrostrictive properties and $\beta$-phase content when compared to a PVDF film. In [6], an electrospun single fiber of PVDF shows a larger piezoelectric coefficient compared to a PVDF film and, therefore, better actuation properties. The actuation capabilities of

* Corresponding author.
*E-mail address:* r.danniballe@rug.nl (R. D'Anniballe).
[1] 0000–0003-1674–8323
[2] 0000–0002-3466–2913
[3] 0000–0002-6051–4332

https://doi.org/10.1016/j.sna.2021.113255

**Table 1**
PVDF-based soft actuators, processed either in thin cast/extruded films or electrospun nanofiber mats.

| Ref. | Configuration | Active material | Evaluated properties | Nanofibers advantages |
|---|---|---|---|---|
| [4] | cantilever beam | electrospun PVDF+CNT | tip displacement, current density | larger actuating displacement (300%) and current density |
| [5] | electrostrictive actuator | electrospun P(VDF-HFP) | strain, current | improved $\beta$-phase content and electrostrictive properties |
| [6] | single electrospun suspended fiber | electrospun PVDF | displacement, piezoelectric coefficient | piezoelectric coefficient twice larger than PVDF thin film |
| [10] | unimorph beam | electrospun P(VDF-TrFE-CTFE) | tip displacement, stiffness | – |
| [11] | linear actuator | electrospun P(VDF-TrFE-CTFE) | force to weight ratio, specific stiffness | higher forces to weight ratio, enhanced stiffening properties |
| [9] | cantilever beam | cast P(VDF-TrFE-CTFE) film doped with CB | dielectric constant/loss, tip displacement | – |
| [7] | multylayered unimorph beam | P(VDF-TrFE-CTFE) film | blocking force, displacement, bending stiffness | – |
| [8] | multylayered unimorph beam | P(VDF-TrFE-CTFE) film with varying cristal fraction | dielectric constant, breakdown strength, tip displacement | – |

films of P(VDF-TrFE-CTFE) have been analyzed in multi-layered unimorph beam [7,8] and in combination with carbon blacks (CB) in a single cantilever beam [9].

To compare electrostrictive actuators, specific parameters that take into account the difference in density in the active layer, either processed by casting/extrusion or electrospinning, are very crucial. Specifically, the sub-micron fibers produced by electrospinning offer various advantages such as high surface area to volume ratio, tunable porosity and, therefore, lower density compared to an homogenoues material [12]. Moreover, the electrospinning process affects the Young's modulus and the dielectric constant of the polymer, which are the main parameters needed to estimate the electrostrictive induced strain [8,13]. By taking into account the differences in density, our previous work on linear soft actuators introduced the force to weight ratio and the specific stiffness to compare extruded films and electrospun nanofibers of P(VDF-TrFE-CTFE) [11].

In this paper, the P(VDF-TrFE-CTFE), processed either as extruded films or electrospun nanofiber mats, is electromechanically characterized and, afterwards, is used as the active layer of unimorph soft actuators. Different thicknesses of the active layer are analyzed to study their influence on the actuation properties, which are evaluated with a designed experimental test set-up. The stiffening properties, the blocking forces, and the mechanical work produced by the actuators are evaluated when direct current (DC) electric fields are applied. To analyze the actuation properties in relation to the morphology of the active layer and to take into account the relative change in density, the specific stiffness and specific work are used [14]. Furthermore, the actuators are stimulated with an alternating current (AC) electric field, and the blocking forces and tip displacements are evaluated. The experiments show a faster viscoelastic relaxation in the nanofibers-based actuators, that can be ascribed to the effect of the electrospinning process on the material properties. Lastly, the current flowing in the actuators during actuation is analyzed, showing a lower leakage current in the case of the nanofiber mats and, therefore, a lower power consumption.

The remainder of the paper is organized as follows. Section 2 presents the materials used in this study, namely the P(VDF-TrFE-CTFE) film and the P(VDF-TrFE-CTFE) electrospun nanofiber mat. Section 3 describes the design of the unimorph cantilever beam soft actuators and the electro-mechanical characterization on the active layers, Section 4 shows the experimental setup and the procedures for the characterization of the soft actuators. The results are reported and discussed in Section 5. The electrical power consumption of the soft actuators is analyzed and discussed in Section 6. Finally, concluding remarks are drawn in Section 7.

## 2. Electro-active material: the P(VDF-TrFE-CTFE)

The polymeric material analyzed in this study is the Solvene T® P (VDF-TrFE-CTFE) (Solvay Specialty Polymers S.p.A., Milano, Italy, www.solvay.com), which is made of 63 mol% of VDF, 28 mol% of TrFE, and 9 mol% of CTFE, and has a Curie temperature of 16°C. The polymer, as reported in the datasheet, has a dielectric permittivity of 45 at 1 kHz.

### 2.1. P(VDF-TrFE-CTFE) films

Three P(VDF-TrFE-CTFE) films have been realized by melt extrusion [15], with an average thickness of ~ 50 $\mu$m, ~ 60 $\mu$m, and ~ 80 $\mu$m. The films have been cut to obtain three specimens (hereafter called F50, F60, and F80), whose dimensions are reported in Table 2.

**Table 2**
Dimensions (length l, breadth b, thickness t, weight w) of the specimens of the P(VDF-TrFE-CTFE) films (i.e., F50, F60, F80) and of the nanofiber mats (i.e., NF50, NF60, NF80).

| Specimen | l [mm] | b [mm] | t [$\mu$m] | w [mg] |
|---|---|---|---|---|
| F50 | 62 | 13 | ~ 50 | 83 |
| F60 | 62 | 13 | ~ 60 | 91 |
| F80 | 62 | 13 | ~ 80 | 127.2 |
| NF50 | 62 | 13 | ~ 50 | 20.3 |
| NF60 | 62 | 13 | ~ 60 | 24.3 |
| NF80 | 62 | 13 | ~ 80 | 32.2 |

### 2.2. P(VDF-TrFE-CTFE) nanofiber mats

The P(VDF-TrFE-CTFE) aligned nanofiber mats have been realized by electrospinning, a nano/micro fabrication technique that has been widely used in many research fields, such as tissue engineering [16], energy harvesting [17] and soft robotics [18]. The process is based on the stretching of a polymeric solution through a high electrostatic field. The system consists of a syringe with a thin metallic needle (loaded with the polymeric solution), a syringe pump to control the flow rate, and a metallic collector positioned at a certain distance. The needle is linked to the positive terminal of a DC power supply, while the collector is grounded [19]. To obtain aligned nanofibers, the metallic collector should either be a plate with recessed steps [20] or a rotating drum [21,22]. The advantages of aligned nanofibers over random ones have been analyzed mainly for PVDF-based sensors and generators [23–25].

For the fabrication of the mats, a solution of P(VDF-TrFE-CTFE) powder (30 wt%) and Acetone:DMF 55:45 (w/w) has been processed by an electrospinning machine (Spinbow™, Bologna, Italy, www.spinbow.it/en), equipped with four needles (length of 55 mm and internal diameter of 0.84 mm) that are connected to 5 mL syringes via polytetrafluoroethylene (PTFE) tubings. The nanofibers have been collected on a rotating drum, covered with poly(ethylene)-coated paper. High rotation speeds of the drum correspond to a great tangential velocity of the drum surface, and consequently, the nanofibers are preferentially packed following that same direction [26]. The parameters of the electrospinning process are summarized in Table 3.

Three P(VDF-TrFE-CTFE) electrospun nanofiber mats have been fabricated, with an average thickness of ~ 50 $\mu$m, ~ 60 $\mu$m, and ~ 80 $\mu$m. To obtain mats of different thickness, the duration of the electrospinning process has been adjusted without modifying the electrospinning parameters. The mats have been cut to obtain three specimens (hereafter called NF50, NF60, and NF80), whose dimensions are reported in Table 2. The thicknesses of the specimens have been measured with a mechanical micrometer (flat steel tip with an area of ~ 30 mm$^2$, sensitivity of 1 $\mu$m), which prevent to sensibly modify the nanofibrous structure. The final values of thickness are the average of several measurements of the different thicknesses along the specimens.

The nanofiber mats have been analyzed by scanning electron microscopy (SEM) with a Phenom ProX Desktop SEM (Thermo Fisher Scientific, Waltham (MA), USA, www.thermofisher.com) and one image of a specimen of aligned nanofibers is shown in Fig. 1a. To quantify the alignment of the fibers, the SEM image was analyzed with the software ImageJ, with the Directionality plugin (ww.imagej.net) [27]. The directionality histogram, as shown in Fig. 1b, reports the amount of fibers as a function of the fiber orientation.

**Table 3**
Electrospinning parameters used for the fabrication of the P(VDF-TrFE-CTFE) nanofiber mats.

| | |
|---|---|
| Flow rate [mL/h] | 0.8 |
| Electric potential [kV] | 26 |
| Drum rotation speed [rpm] | 2430 |
| Distance needles-drum [cm] | 14 |
| Relative humidity [%] | 52 |
| Temperature [°] | 20 |

## 3. The P(VDF-TrFE-CTFE)-based actuators

The P(VDF-TrFE-CTFE)-based actuators are designed as asymmetric unimorph cantilever beams [10]. In particular, they consist of an active layer of P(VDF-TrFE-CTFE), either extruded film or aligned nanofiber mat with dimensions as reported in Table 2, interleaved between two conductive electrodes of aluminum, and held together by a passive polyethylene adhesive tape on one side and a passive Kapton® tape on the other side. The unimorph structure is sketched in Fig. 2 and the dimensions of the passive layers are reported in Table 4.

When an external electric field is applied across the P(VDF-TrFE-CTFE), a strain is produced in its longitudinal axis due to the synergistic effect of the Maxwell stress (i.e., the electrodes are attracted to each other and, as a consequence, the P(VDF-TrFE-CTFE) is mechanically compressed in the thickness direction and expands in the longitudinal directions) and the electrostriction (i.e., the applied electric field induces a conformation change of the polymeric chains that may produce a large strain in thickness) [13]. The passive layers, with their different elastic moduli, resist the deformation, resulting into the bending of the actuators [28].

When an electric field $E$ is applied to the P(VDF-TrFE-CTFE), a total strain $S$ is induced in the material, given by:

$$S = S_{Maxwell} + S_{electrostriction} = -\frac{1}{2}\frac{\epsilon_0 \epsilon_r E^2}{Y} + QP'^2 \quad (1)$$

where $Y$ is the P(VDF-TrFE-CTFE) Young's modulus, $\epsilon_r$ is the polymer dielectric constant, $\epsilon_0$ is the vacuum permittivity, $Q$ is the electrostrictive coefficient, and $P'$ is the phase transformation-induced polarization. However, when the electrodes are bonded to the polymers surface, the electrostrictive effect is negligible for values of electric field below the P(VDF-TrFE-CTFE) activation field (i.e., 50 MV/m) [13], since the phase transformation can hardly take place. As a consequence, the electric field induced strain in this electromechanical characterization is mainly due to the Maxwell stress. Therefore, as described by Equation 1, the Young's modulus and the dielectric constant of the active layer are the two main parameters for the evaluation of the actuators performances.

### 3.1. Electro-mechanical characterization of the active layer of the P(VDF-TrFE-CTFE)-based actuators

#### 3.1.1. Young's Modulus

The Young's moduli of the P(VDF-TrFE-CTFE) films and nanofiber mats have been evaluated in tensile tests with the test instrument ElectroPuls E1000 (Instron™, Norwood (MA), USA, www.instron.us), which is equipped with a 5N Instron™ static load cell 2530–5N. A specimen (either of the film or of the nanofiber mat) is placed in the test instrument by following the procedure proposed in [11,29] to avoid any damage to the material. First, the specimen is anchored into a paper frame with a bi-adhesive tape to prevent slippage. Then, the paper frame is clamped by means of two 3D-printed ABS clamps in the test instrument and, afterwards, the paper frame is cut on the sides, leaving the specimen properly placed in the test instrument.

For the aligned electrospun nanofibers, the elastic modulus is evaluated along the alignment direction and perpendicularly to the alignment direction to analyze the orthotropic elastic properties of

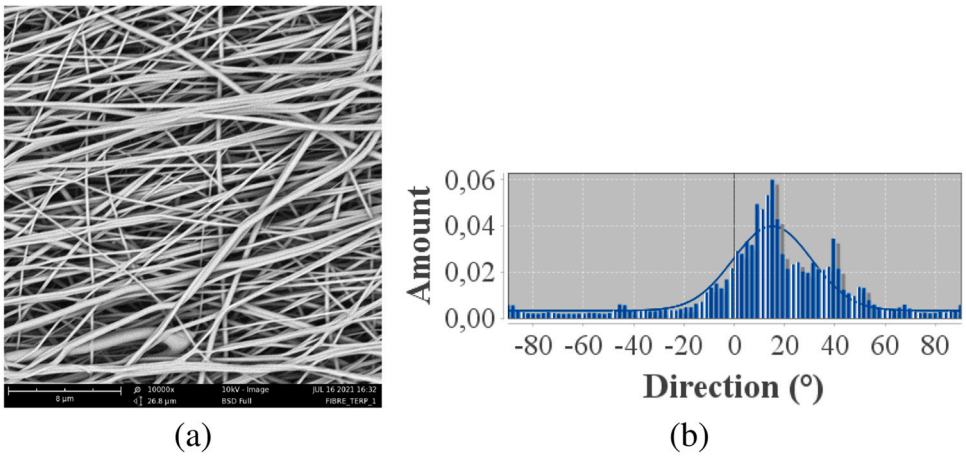


**Fig. 1.** SEM image of one specimen of the aligned nanofiber mat (a) and directionality histogram (b).

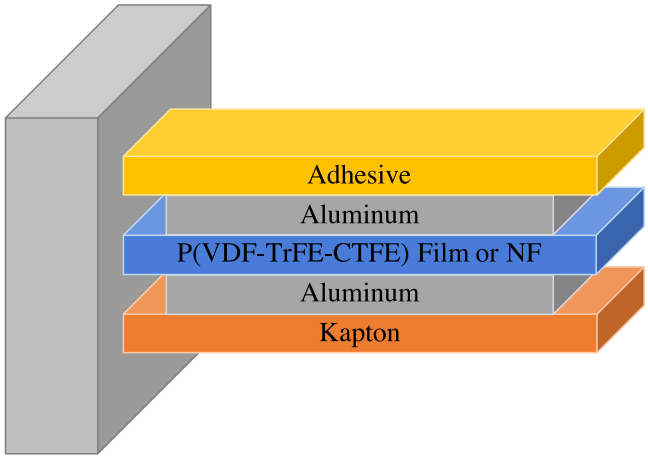


**Fig. 2.** The P(VDF-TrFE-CTFE)-based actuators as unimorph cantilever beams.

**Table 4**
Dimensions (length l, breadth b, thickness t, weight) of the passive layers of the P(VDF-TrFE-CTFE)-based actuators.

| Material | l [mm] | b [mm] | t [$\mu$m] |
|---|---|---|---|
| Kapton® tape | 63 | 13 | ~ 57 |
| Polyethylene tape | 63 | 13 | ~ 50 |
| Aluminium tape | 61 | 12 | ~ 55 |

the aligned nanofiber mats. Each tensile test has been repeated on three different samples and the Young's moduli are evaluated as the slope of the tangent to the stress-strain curve at low strain, as reported in Fig. 3.

The Young's modulus of the P(VDF-TrFE-CTFE) film is 124 MPa (standard deviation of 3.96 MPa), the Young's modulus of the P(VDF-TrFE-CTFE) nanofiber mat in the aligned direction is 32.49 MPa (standard deviation of 5.40 MPa) and in the direction perpendicular to the alignment is 3.40 MPa (standard deviation of 0.79 MPa).

### 3.1.2. Dielectric constant

The dielectric constant of the P(VDF-TrFE-CTFE) nanofiber mat has been evaluated with the Alpha dielectric analyzer (Novocontrol Technologies GmbH & Co. KG, Montabaur, Germany, www.novocontrol.de). The real part of the dielectric constant is reported in Fig. 4 for different frequencies, where it can be noted that the dielectric constant decreases when the frequency increases. This is because the dipoles of the dielectric materials cannot follow rapid changes in the field direction [30]. The dielectric constant of the P(VDF-TrFE-CTFE) nanofibers is equal to 2.3 at 1 kHz. The value of the dielectric constant for the nanofiber mat is significantly lower compared to the one of the extruded film evaluated at the same frequency. This is due to the high porosity of the electrospun nanofiber mat [31], i.e., the mat can be considered as a two-phase mixture composite, in which air ($\epsilon_r = 1$), is dispersed in the nanofiber matrix. Therefore, the resulting dielectric constant is given by the contribution of the two phases. All the nanofiber mats produced and used for the actuators are characterized by a comparable porosity

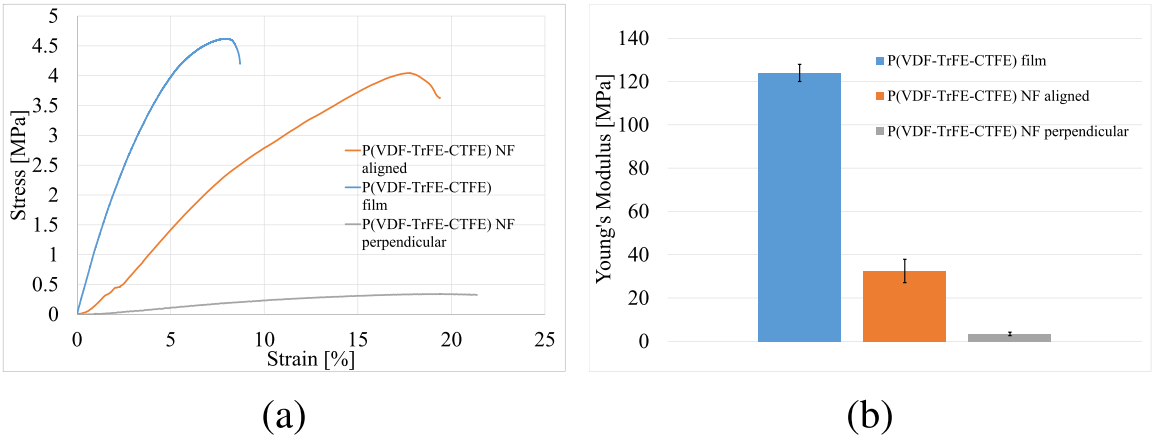


**Fig. 3.** Stress-strain graph (a) and Young's moduli (mean and standard deviation) (b) of the P(VDF-TrFE-CTFE) films and nanofiber mats.

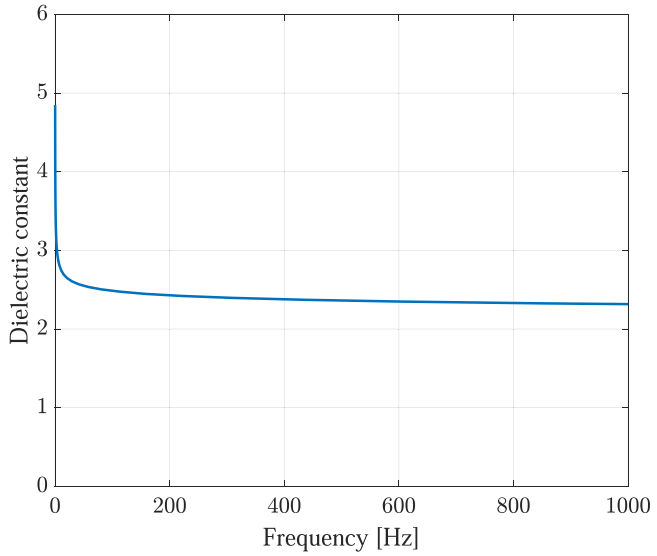


**Fig. 4.** Dielectric constant evaluated at different frequencies.

(~70%) and, therefore, the reported measurement of the dielectric constant can be applied to all the analyzed nanofibers-based actuators.

## 4. Electro-mechanical characterization of the P(VDF-TrFE-CTFE)-based actuators

This Section describes the experimental test set-up and the electro-mechanical characterization of the P(VDF-TrFE-CTFE)-based soft actuators.

The test set-up consists of the test instrument ElectroPuls E1000, equipped with the 5N Instron™ static load cell 2530–5N and an optical encoder. A 10/10B-HS high-voltage amplifier (Trek Inc., Lockport, New York, USA, www.trekinc.com) is connected through crocodile plugs to the aluminum electrodes of the soft actuator and is operated through the DG1022 waveform generator (RIGOL Technologies, Beaverton, Oregon, USA, www.rigolna.com). The Instron™ Wavematrix software records both the forces measured by the load cell and the applied voltages. In the test instrument, the soft actuator is held at one extremity by a support, designed and 3D printed in ABS material, while the other extremity is free to move and, when in contact with the load cell, the force exerted by the actuator can be measured. The 3D printed support is rigidly connected to the linear motor of the test instrument so that its position can be changed. Fig. 5 shows the overall test set-up and Fig. 6 shows how the soft actuator is mounted in the test instrument.

### 4.1. Force-deflection

To measure the force-deflection characteristics, the experiment is performed as follow and repeated for different values of applied electric field:

- The soft actuator is fixed in the 3D printed support, and, thanks to the gravity and the applied electric field, it bends until the tip touches the load cell (i.e., zero deflection position).
- After 10 s since the application of the electric field, the forces produced by the actuators are measured with the load cell and recorded with the Wavematrix software. Waiting 10 s after the voltage application ensures that the recorded forces are in a steady state during the entire experiment [10].

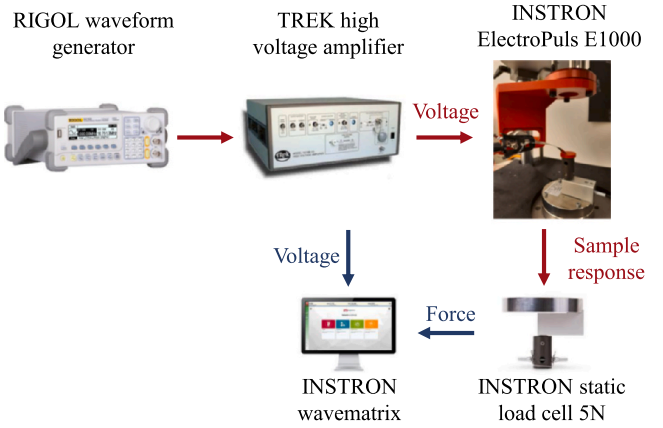


**Fig. 5.** Experimental test set-up for the electromechanical characterization of the P(VDF-TrFE-CTFE)-based soft actuators. The TREK 10/10B-HS high-voltage amplifier, operated through the RIGOL DG1022 waveform generator, applies a voltage to the actuator, which is placed in the Intron ElectroPuls E1000. The forces exerted by the specimen is measured by the Instron load cell and recorded by the Instron™ Wavematrix software.

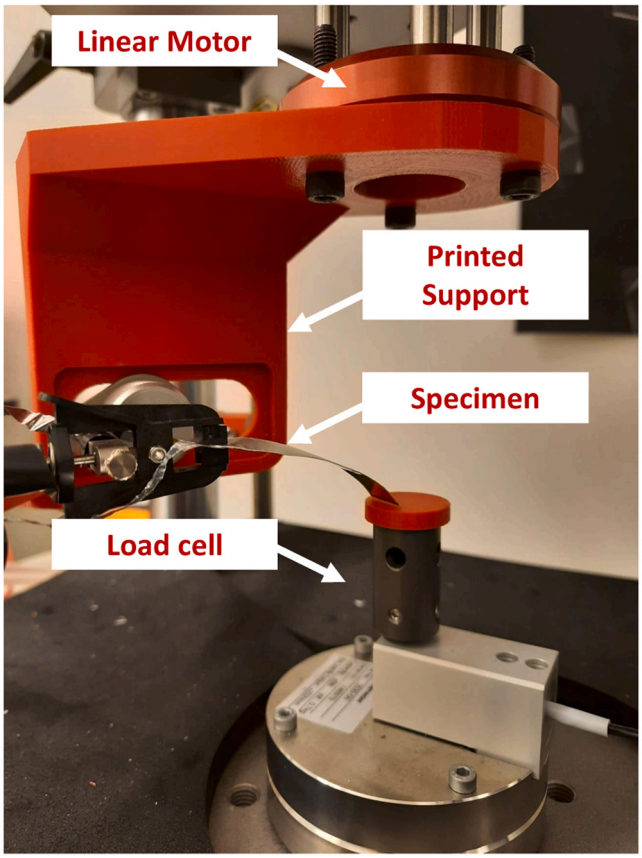


**Fig. 6.** The set-up for the experimental test to measure the forces exerted by the P(VDF-TrFE-CTFE)-based actuators.

- The linear motor is then moved downwards up to 5 mm with steps of 0.5 mm, and the forces applied by the tip of the actuator are measured and registered.

To ensure repeatability, this test is performed three times on each actuator for four different values of applied electric field. Thanks to this characterization, it is possible to obtain the force-deflection curve at different applied electric field, where the slope of this curve

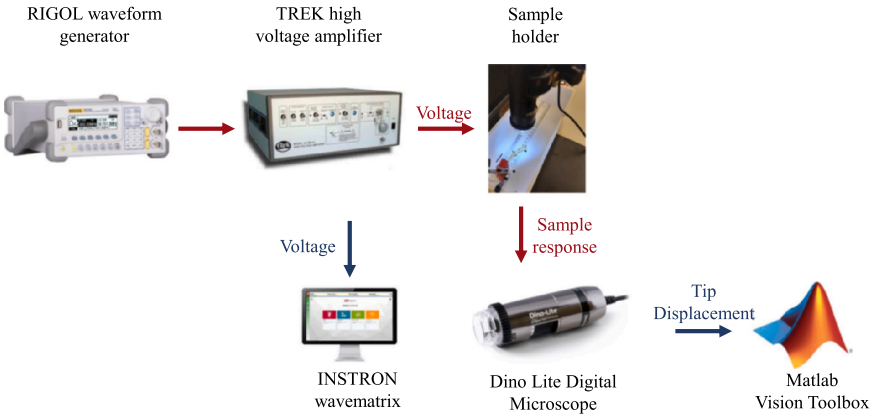


**Fig. 7.** Test setup for the measurement of the tip deflection of the soft actuators. The TREK 10/10B-HS high-voltage amplifier, operated through the RIGOL DG1022 waveform generator, applies a voltage to the actuator, which is placed in the Intron ElectroPuls E1000. The tip deflection is captured with the digital m7915mztl 5 MPx microscope and processed in Matlab.

represents the bending stiffness of the actuator for each value of the applied electric field.

### 4.2. Blocking force

The same test set-up is used for the evaluation of the actuators' blocking force, which represents the amount of force required to prevent the deflection of the actuator [32,33]. To calculate the blocking force, the linear motor of the test instrument is kept at a fixed position, and the forces produced by the tip of the actuator are recorded when different values of electric field are applied. The actuator is placed in the 3D printed support and, thanks to the gravity, it bends until the tip touches the load cell (i.e., zero deflection position). Then, different electric fields are applied to the actuator and the forces exerted by the tip are registered.

### 4.3. Tip deflection

A digital m7915mztl 5 MPx microscope (Dino-Lite, AnMo Electronics Corp, Taipei, Taiwan, www.dino-lite.com) is used to record the deflection of the tip of the actuators, when stimulated by different electric fields. The deflection is recorded in a video with the DinoCapture software (version 2.0) which is, then, analyzed in Matlab (Mathworks, USA, www.mathworks.com). Fig. 7 shows the overall experimental test set-up for the measurement of the tip deflection.

## 5. Results and discussion

### 5.1. Force-deflection and specific stiffness

Fig. 8 shows the force-deflection plots of the film-based actuators (left) and of the nanofiber-based actuators (right), when stimulated by different electric fields. The data obtained from the force-deflection experiments are linearly interpolated for every applied electric field.

From the plots, it can be observed that the higher the applied electric field, the higher the generative forces are for a certain imposed displacement. This means that the actuators get stiffer as the electric field increases. From the slope of the linear interpolation, it is possible to derive the bending stiffness and the stiffening of the actuators when an electric field is applied. The stiffening is calculated as the percentage increase of the stiffness for different electric fields with respect to the stiffness of the actuators without any applied field, which are reported in Table 5 for the film-based actuators and in Table 6 for the nanofibers-based actuators.

The values of stiffening showed in Tables 5 and 6 can be normalized to the actuators total weight (both active layers and passive layers are considered), to define the specific stiffening at different values of applied electric field, as reported in Table 7. From the Table, it can be noted that the nanofibers-based actuators show an overall higher specific stiffening for the analyzed applied electric field.

#### 5.1.1. Specific work

Fig. 9 shows the working area of the actuators, which is represented in the force-deflection plane by the area between the minimum stiffness line (i.e., without any applied electric field) and the maximum stiffness line (i.e., computed at 15 MV/m).

It can be noted that the area is comparable for all the analyzed actuators. However, the thickness of the active layer has an effect on it. In fact, when the active layer thickness increases, the working area is shifted to higher values in the force-deflection plane. Therefore, it should be highlighted that the thickness of the active layer is an important parameter when designing a soft actuator with variable stiffness. The work produced by the actuators, i.e., the area in the force-deflection plots, can be calculated in mN × mm from Fig. 9 [34]. The force-deflection experiment, as described in Section 4.1, is performed by applying a static DC electric field, with the forces evaluated at steady-state during the entire experiment. The work produced by the actuators are reported in Table 8, in which the obtained values are divided by the actuators' total weight to define the work produced for mg of material, i.e., the actuators specific work [35].

It can be noticed that, for all the analyzed actuators, the specific work is higher for the nanofibers-based actuators.

### 5.2. Blocking force

Fig. 10 shows the plots of the blocking forces of the film-based actuators (left) and of the nanofibers-based actuators (right), when stimulated by a repeated 15 MV/m square electric field.

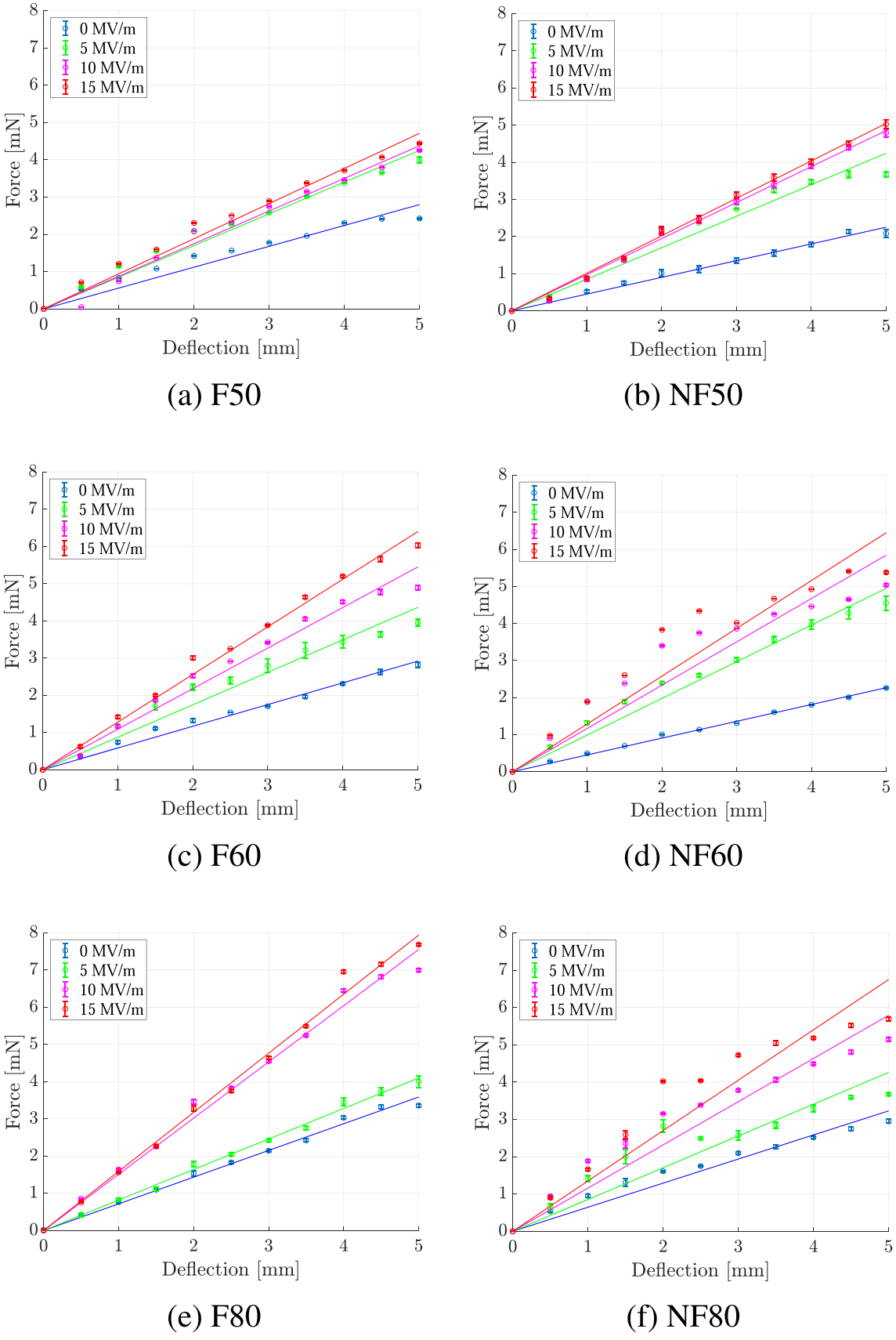


**Fig. 8.** Force-deflection of the P(VDF-TrFE-CTFE)-based actuators, when stimulated by different magnitudes of the electric field. Mean and standard errors are reported in the plots.

**Table 5**
Bending stiffness and % stiffening of the film-based actuators, when stimulated by different electric fields.

| Actuator | Electric field [MV/m] | Stiffness [mN/mm] | Stiffening [%] |
|---|---|---|---|
| F50 | 0 | 0.477 | – |
| F50 | 5 | 0.768 | 61.11 |
| F50 | 10 | 0.883 | 85.28 |
| F50 | 15 | 0.942 | 97.45 |
| F60 | 0 | 0.545 | – |
| F60 | 5 | 0.766 | 40.41 |
| F60 | 10 | 1.042 | 90.94 |
| F60 | 15 | 1.233 | 125.92 |
| F80 | 0 | 0.697 | – |
| F80 | 5 | 0.819 | 17.41 |
| F80 | 10 | 1.460 | 109.31 |
| F80 | 15 | 1.599 | 129.28 |

**Table 6**
Bending stiffness and % stiffening of the nanofiber mats-based actuators, when stimulated by different electric fields.

| Actuator | Electric field [MV/m] | Stiffness [mN/mm] | Stiffening [%] |
|---|---|---|---|
| NF50 | 0 | 0.429 | – |
| NF50 | 5 | 0.793 | 79.86 |
| NF50 | 10 | 0.989 | 124.33 |
| NF50 | 15 | 1.027 | 132.98 |
| NF60 | 0 | 0.441 | – |
| NF60 | 5 | 0.894 | 102.76 |
| NF60 | 10 | 0.945 | 114.26 |
| NF60 | 15 | 1.055 | 139.24 |
| NF80 | 0 | 0.557 | – |
| NF80 | 5 | 0.676 | 21.31 |
| NF80 | 10 | 0.965 | 73.08 |
| NF80 | 15 | 1.114 | 105.79 |

From the plots, it is possible to derive the maximum blocking force (mean and standard error), which are reported in Fig. 11 for the film-based actuators (left) and the nanofibers-based actuators (right). It can be noted that the film-based actuators, characterized by higher bending stiffness values compared to the nanofibers-based actuator (see Section 5.1), produce higher forces when stimulated by the same applied electric field. Furthermore, from Fig. 10, it can be noted that the actuators exhibit a nonlinear viscoelastic behavior [10] and, more specifically, that the blocking force consists of a nonlinear instantaneous elastic response and a slower viscous response. In response to an electromechanical load, in fact, an elastomer may evolve toward a new state of equilibrium by various dissipative processes. Subject to a mechanical force and an electric field, the polymer takes time to equilibrate to its state of kinematic deformation and charge polarization. The relaxation process is mainly affected by two factors, i.e., the entangled polymer chains and the dielectric relaxations [36].

**Table 7**
Specific stiffening of the P(VDF-TrFE-CTFE) based actuators, when stimulated by different magnitudes of the electric field.

| Active layer thickness [$\mu$m] | Electric field [MV/m] | Film based specific stiffening [%/mg] | Nanofibers based specific stiffening [%/mg] |
|---|---|---|---|
| 50 | 0 | – | – |
| 50 | 5 | 0.17 | 0.29 |
| 50 | 10 | 0.24 | 0.44 |
| 50 | 15 | 0.27 | 0.47 |
| 60 | 0 | – | – |
| 60 | 5 | 0.11 | 0.36 |
| 60 | 10 | 0.25 | 0.40 |
| 60 | 15 | 0.34 | 0.48 |
| 80 | 0 | – | – |
| 80 | 5 | 0.04 | 0.07 |
| 80 | 10 | 0.27 | 0.24 |
| 80 | 15 | 0.32 | 0.35 |

**Table 8**
Maximum work output and specific work.

| Actuator | Work [mN*mm] | Specific work [ (mN*mm)/mg] |
|---|---|---|
| F50 | 4.777 | 0.0133 |
| F60 | 8702 | 0.0238 |
| F80 | 10.881 | 0.0271 |
| NF50 | 7 | 0.0237 |
| NF60 | 10.445 | 0.0350 |
| NF80 | 8.810 | 0.0287 |

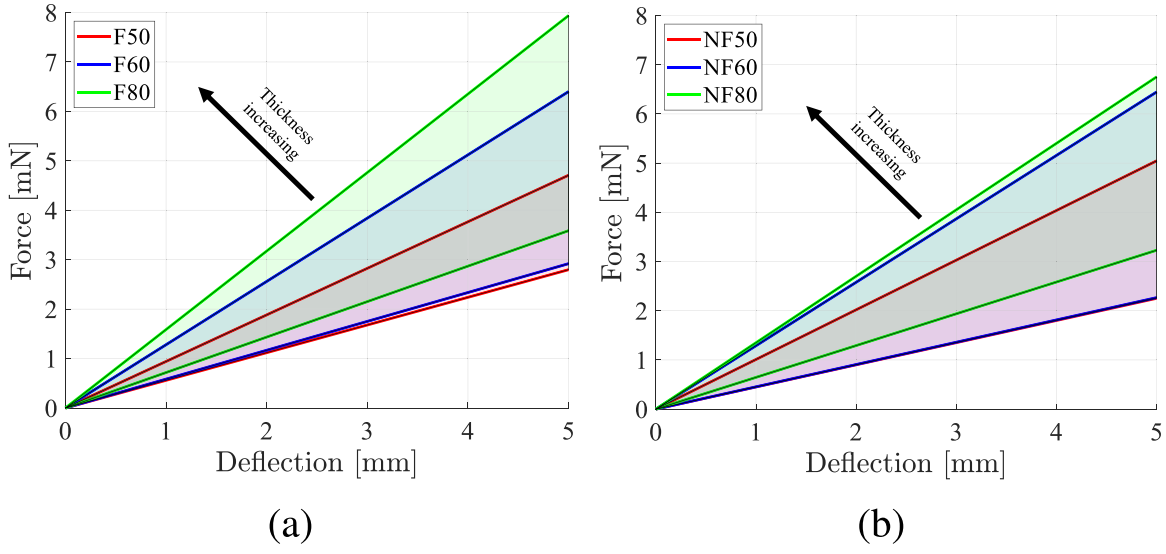


**Fig. 9.** Working area for the (a) film-based actuators and (b) nanofibers-based actuators.

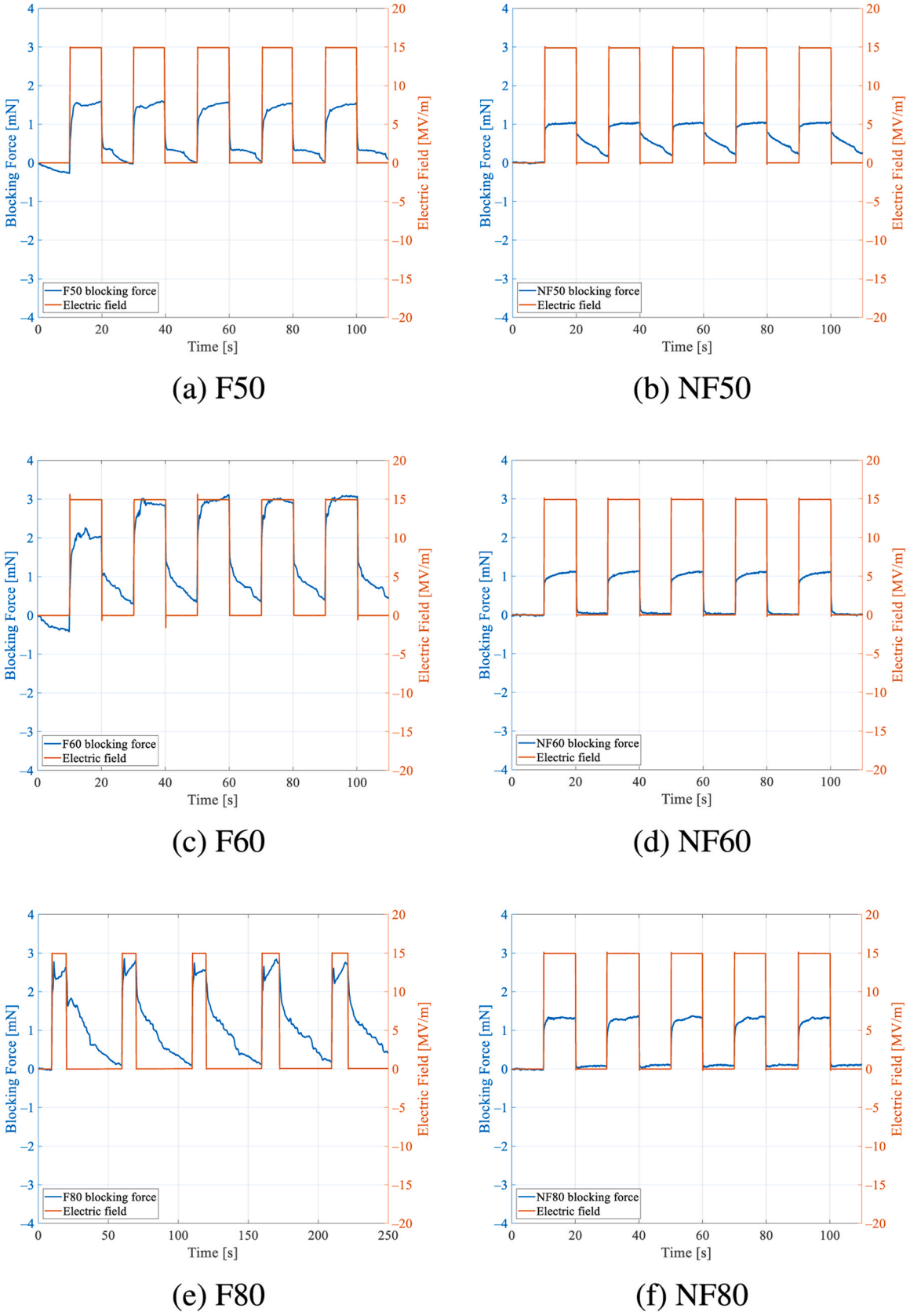


**Fig. 10.** Blocking forces of the P(VDF-TrFE-CTFE)-based actuators, when stimulated by 15 MV/m square electric fields.

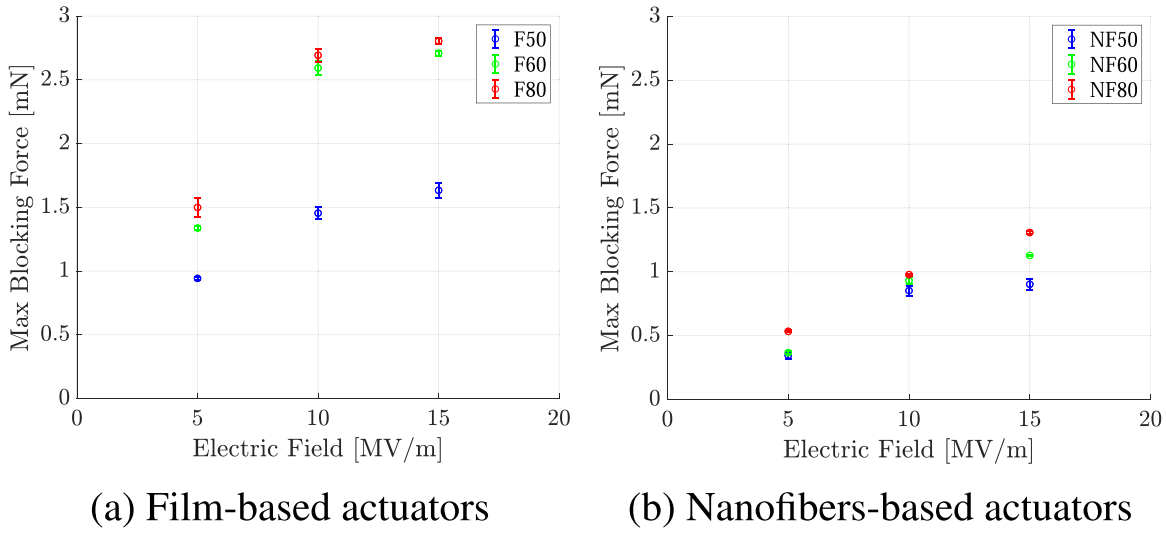


**Fig. 11.** Blocking forces of the P(VDF-TrFE-CTFE)-based actuators, when stimulated by different applied electric fields.

When a force is applied to the polymer, the viscoelastic relaxation may be caused by slipping and sliding among polymer chains and rotation of joints among monomers. Moreover, subjected to an electric field, the polymer relaxes to a new state of polarization over a characteristic time and the process of re-orientation of the molecular dipoles in a polar dielectric is called dielectric relaxation. Viscoelastic hysteresis has been shown to exert an adverse effect on actuators performances and cause positioning inaccuracy [37]. In order to further investigate the viscous responses of the actuators, a sinusoidal electric field of 15 MV/m and 0.2 Hz frequency is applied and the resulting blocking forces are plotted in Fig. 12. It can be observed that, as expected from Equation 1, the blocking forces produced by the actuators are independent from the polarity of the electric field. Moreover, it can be noted that the nanofibers-based actuators reach almost a fully relaxation (i.e., forces equal to zero) when the applied electric field decreases to zero. Consequently, in the generated sinusoidal forces, the peak to peak amplitude is close to the wave maximum amplitude and, therefore, to the maximum forces generated by the actuators. On the contrary, it is possible to notice that the film-based actuators do not reach a full relaxation when the applied electric field is equal to zero. Fig. 13 shows the results of the characterization for the film-based actuators (left) and for the nanofibers-based actuators (right) in terms of the maximum generated force, peak to peak force, and normalized peak to peak force, which expresses in percentage the ratio between the maximum force and the peak to peak force and, therefore, it gives information on the velocity of the relaxation.

From the normalization shown in Fig. 13e and f it can be noted that:

- The normalization values are lower for the film-based actuators.
- The normalization values decrease with the increasing of the active layer thickness for the film-based actuators.
- The active layer thickness does not have any influence on the normalization and, therefore, on the relaxation for the nanofibers-based actuators.

It is possible to conclude that the nanofibers-based actuators, characterized by lower density compared to the film-based actuators, have a faster viscous relaxation and, therefore, a faster dynamics.

### 5.3. Tip deflection

Fig. 14 shows the plots of the tip deflection of the film-based actuators (left) and the nanofibers-based actuators (right), when stimulated by a sinusoidal electric field of 15 MV/m at 0.1 Hz.

Considering that the unimorph actuation is dependent on the transmission of shear force from the active to passive material, smaller displacements occur with actuators consisting of thicker active layers [38], as can be noted in Fig. 15, where the results of the experiments are summarized. It can be noticed that the maximum tip deflection produced by the actuators, with the same active layer thickness, is higher for the nanofibers-based actuator (Fig. 15b), as expected from the actuators lower bending stiffness as shown in Section 5.1. A normalization of the results is performed here. The normalization values are lower in percentage compared to the results shown in Section 5.2, most likely for the effect of air friction that affects the actuators dynamic. However, also in the tip deflection experiments, the nanofibers-based actuators show higher values of normalization (Fig. 15f) compared to the film-based actuators (Fig. 15e).

Electrospinning is a process that modifies the material properties for the following main reasons [11]: (i) the mechanical stretching enforced by the electrospinning process enables for the alignment of the polymeric chains in the amorphous phase; (ii) the nanofibers have dipoles with a self-induced orientation; (iii) the electrical

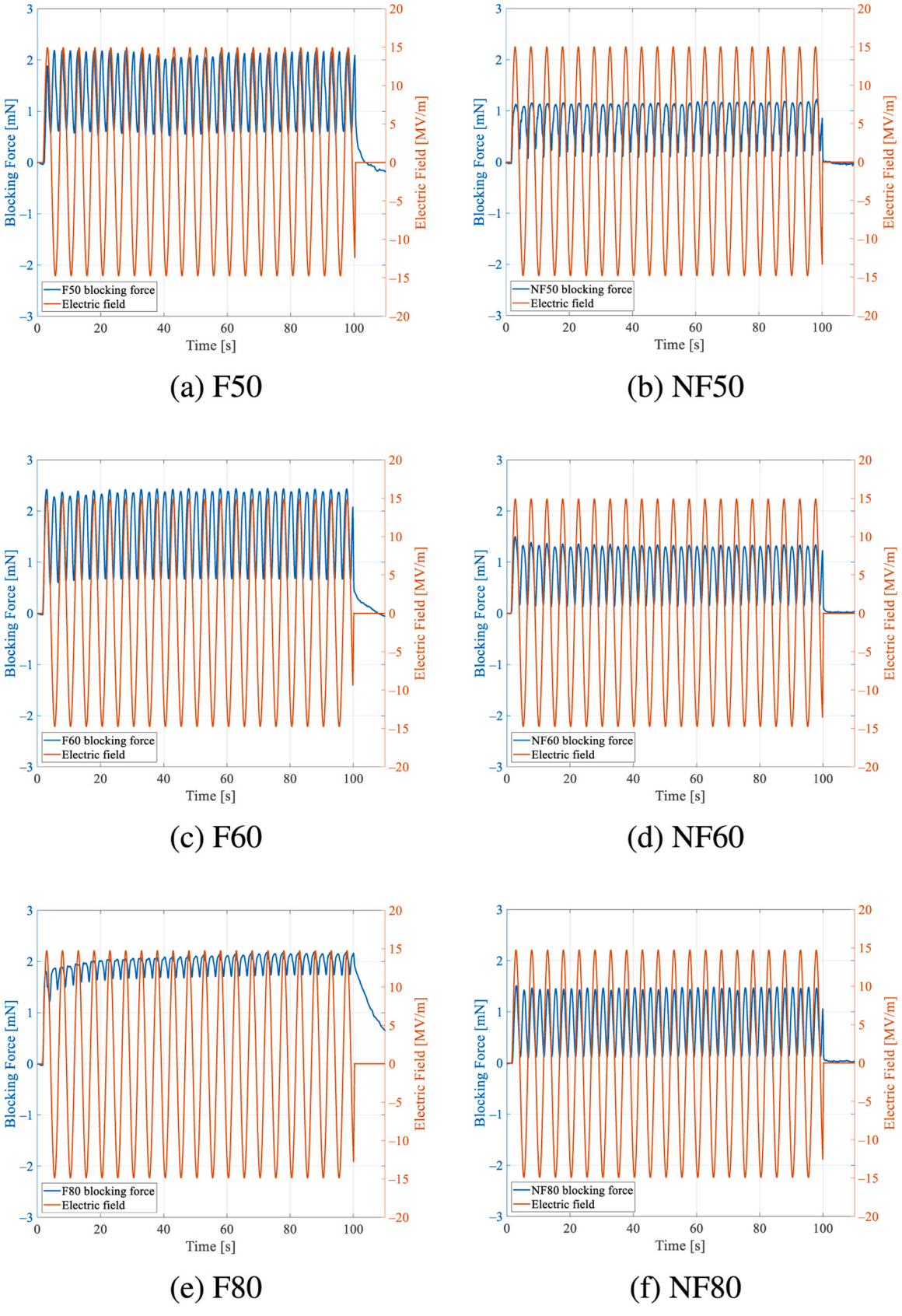


**Fig. 12.** Blocking forces of the P(VDF-TrFE-CTFE)-based actuators, when stimulated by a sinusoidal electric field of 15 MV/m at 0.2 Hz.

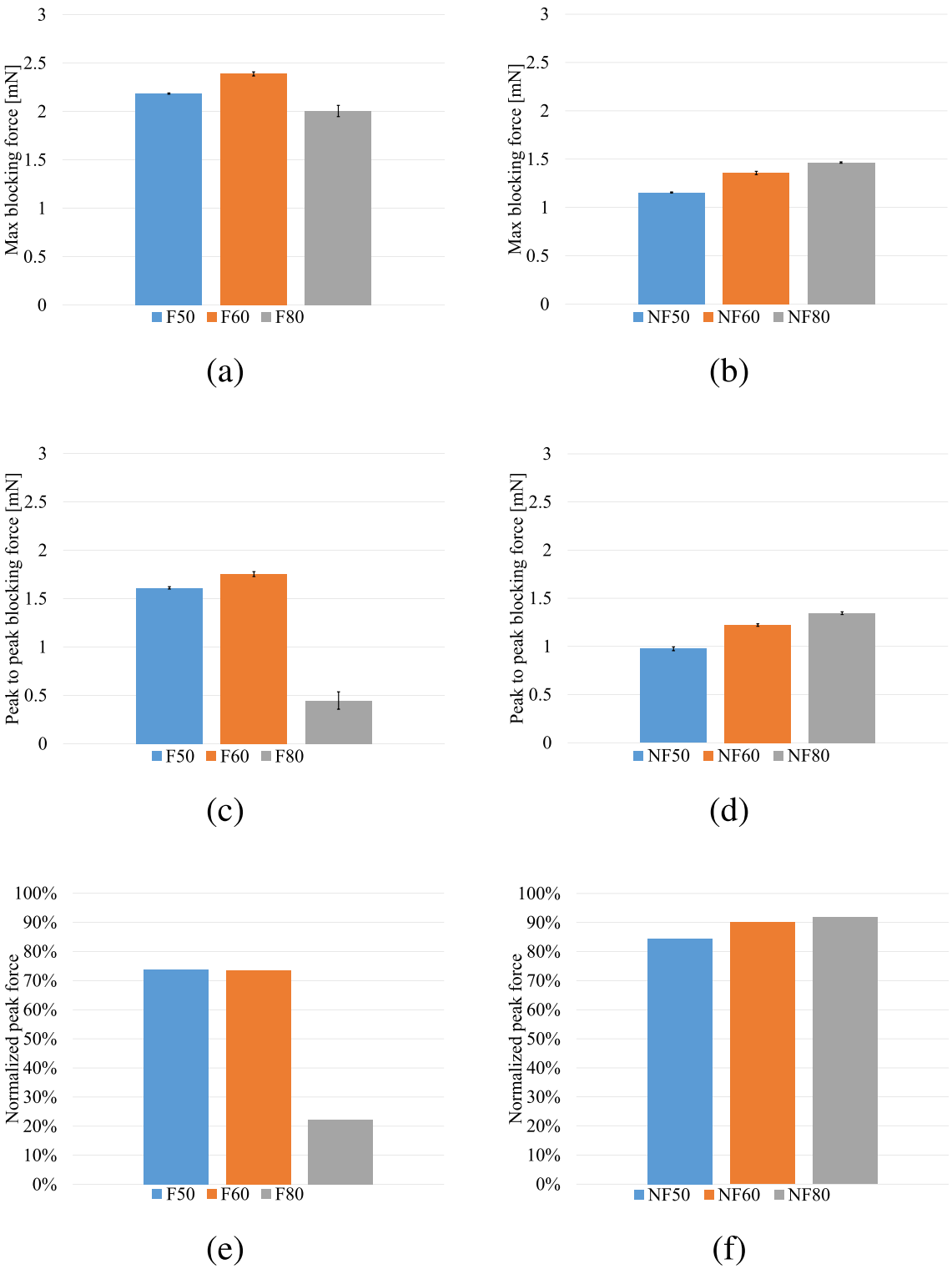


**Fig. 13.** Maximum blocking force (mean ± standard error) for (a) film-based actuators and (b) nanofibers-based actuators. Peak to peak blocking force (mean ± standard error) for (c) film-based actuators and (d) nanofibers-based actuators. Normalized peak to peak force (in percentage) on the max blocking force for (e) film-based actuators and (f) nanofibers-based actuators, when stimulated by a sinusoidal electric field of 15 MV/m at 0.2 Hz. Mean and standard errors are calculated for each actuator on the peaks of the sinusoidal blocking forces.

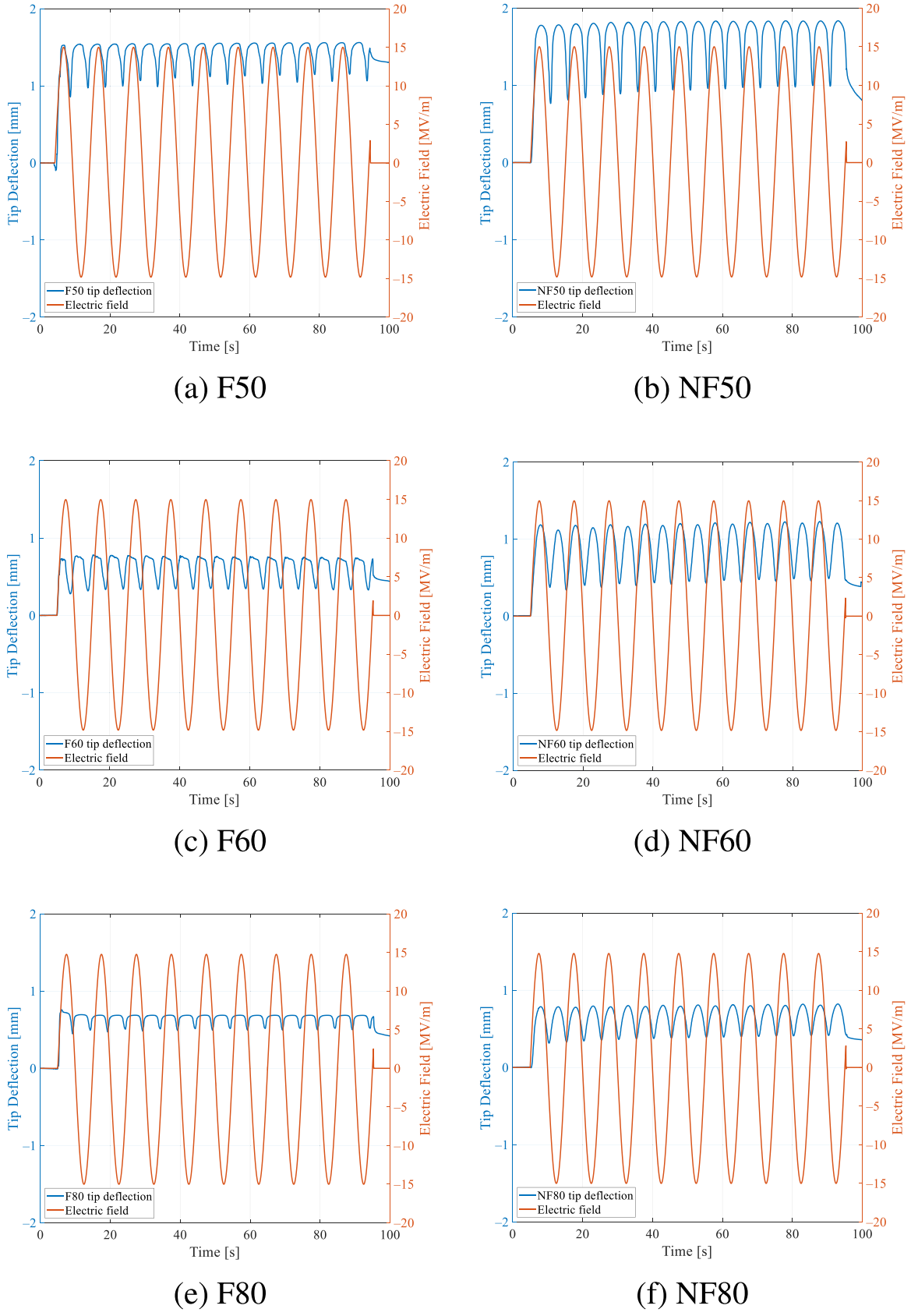


**Fig. 14.** Tip deflections of the P(VDF-TrFE-CTFE)-based actuators, when stimulated by sinusoidal electric fields of 15 MV/m at 0.1 Hz.

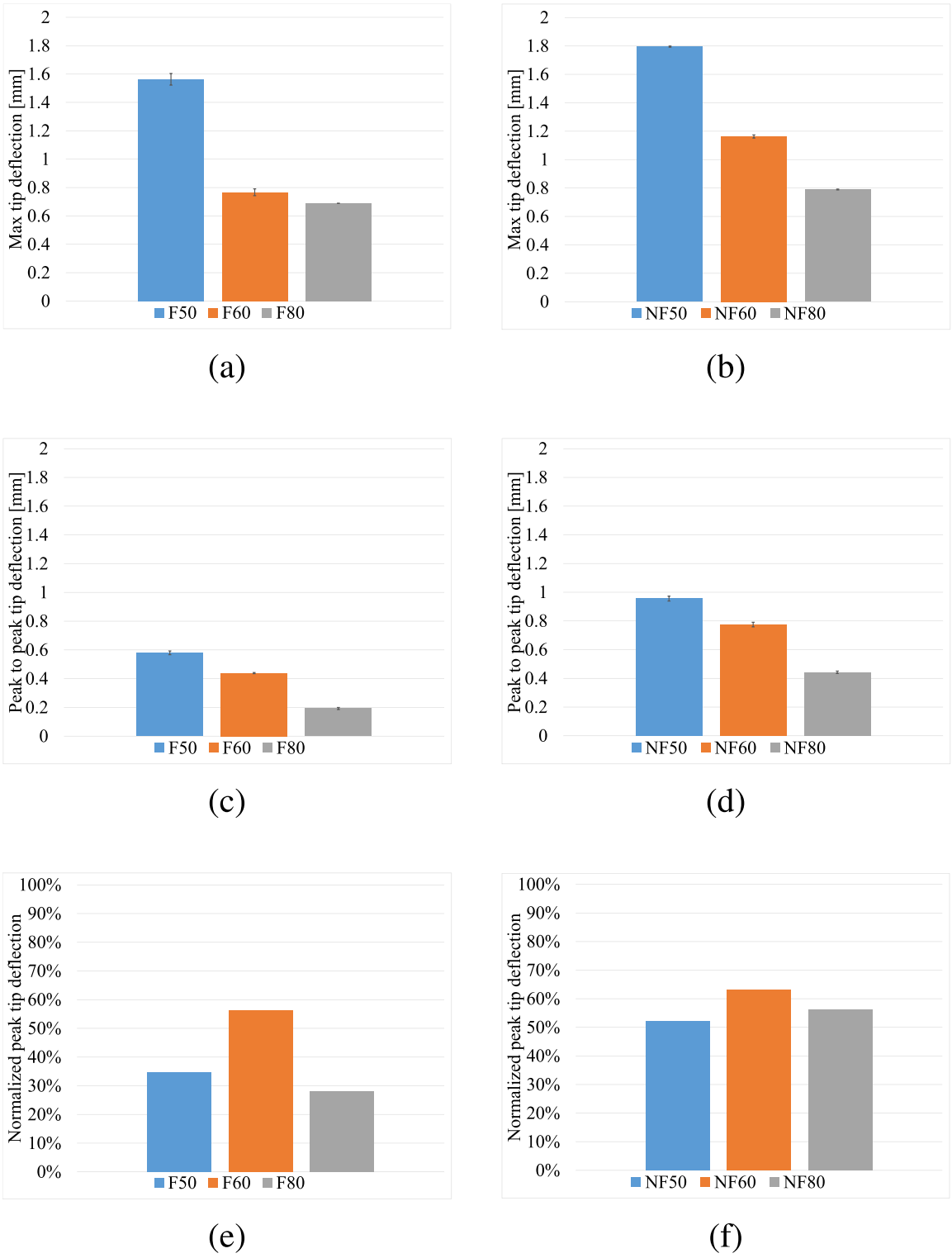


**Fig. 15.** Maximum tip deflection (mean ± standard error) for (a) film based actuators and (b) nanofibers based actuators. Peak to peak deflection (mean ± standard error) for (c) film-based actuators and (d) nanofibers-based actuators. Normalized peak to peak deflection (in percentage) on the max tip deflection for (e) film-based actuators and (f) nanofibers-based actuators, when stimulated by a sinusoidal electric field of 15 MV/m at 0.1 Hz. Mean and standard errors are calculated for each actuator on the peaks of the sinusoidal tip deflection.

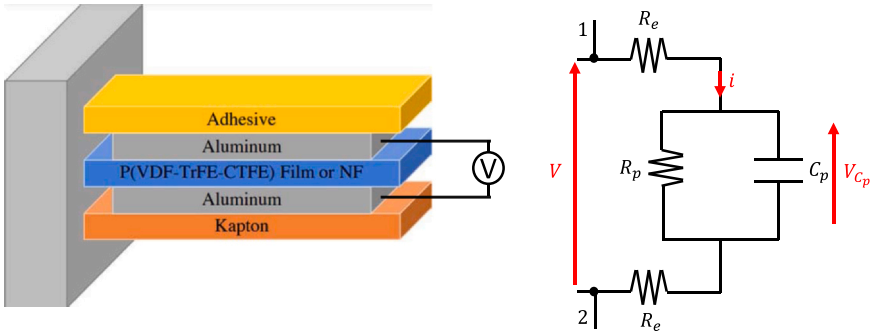


**Fig. 16.** Equivalent electrical circuit of the actuators
Adapted from [42].

poling also enforced by the electrospinning process enables the spontaneous dipolar orientation [5] inside the nanofibers; and (iv) the nanofibers have a larger surface area to volume ratio than a bulk. Furthermore, nanofibers allow for a better alignment of the dipoles because of the smaller amount of material that has to be reorganized around each dipole. The described properties may have a direct influence on the relaxation process, reducing the relaxation time of the nanofibers based P(VDF-TrFE-CTFE) and improving the actuator performances. Many studies for dielectric actuators shows that prestretching provides benefits such as a shorter relaxation time and reduced drifting effects [39,40]. The electrospinning process provides a mechanical and electrical stretching in the polymer production phase, contributing in the faster relaxation.

## 6. Electrical power consumption

The use of high voltage to actuate the electrostrictive P(VDF-TrFE-CTFE) leads inevitably to the flowing of leakage currents [41]. When a dielectric is connected to a power source, a small current may flow through the dielectric. This process is known as current leakage and is a result of the transport of electrons, ions, or both, and is often linked to the presence of impurities and imperfections [36]. Fig. 16 shows the equivalent electrical circuit for the analyzed actuators, where $V$ is the applied voltage, $i$ is the total flowing current, $C_p$ is a capacitance that represents the charge stored in the polymer, $R_p$ is a resistor that represents the current leakage path through the polymer, and $R_e$ represents the surface resistance associated to the electrodes.

To compare the flowing current in the case of film- and nanofibers-based actuators, it is possible to neglect the surface resistance of the electrodes, since both the actuators are made with the same configuration. According to the principle of charge conservation, the current is the sum of the charge flow rate to the capacitor $Q_p$ and the current leakage through the resistor. By applying Kirchhoff's laws and expressing the relationships of the electric components in complex form ($I_{C_p} = Vi\omega C_p$; $I_{R_p} = V/R_p$), the total equivalent impedance can be simply written as:

$$Z_p = \frac{R_p}{i\omega C_p R_p + 1} \tag{2}$$

Following the Ohm's law, the current can be expressed as:

$$i(t) = \frac{i\omega C_p R_p + 1}{R_p} V(t) \tag{3}$$

with $C_p = \epsilon_r \epsilon_0 S/d$, with S that represents the area and d the thickness of the polymer. To analyze the flowing of current, a sinusoidal electric field of 15 MV/m and frequency of 0.1 Hz, is applied and, through the voltage amplifier, the current is monitored and Fig. 17 shows the plots of the film-based actuators (left) and the nanofibers-based actuators (right).

The peak values of current for the analyzed actuators are summarized in Fig. 18.

It can be noted that for the nanofibers based actuators the flowing current is around one order of magnitude lower compared to the film based actuators. This is described by Equation 3, in which the capacitance of the active layer and, more specifically, its dielectric constant is proportional to the flowing current. Therefore, the higher dielectric constant of the film leads to higher values of currents. From the graphs, it is possible to evaluate the electrical instantaneous power consumption $P_{peak}$:

$$P_{peak} = V(t)i(t) \tag{4}$$

and the electrical average power consumption $P_{avg}$ that can be evaluated as:

$$P_{avg} = \frac{1}{T}\int_0^T V(t)i(t)dt = V_{RMS} I_{RMS} cos(\phi) \tag{5}$$

where $V_{RMS}$ and $I_{RMS}$ are the root mean square values of voltage and current and $cos(\phi)$ represents the power factor. The results are shown in Table 9.

As expected, the electrical power consumption is one order of magnitude lower in the case of the electrospun nanofibers based-actuators.

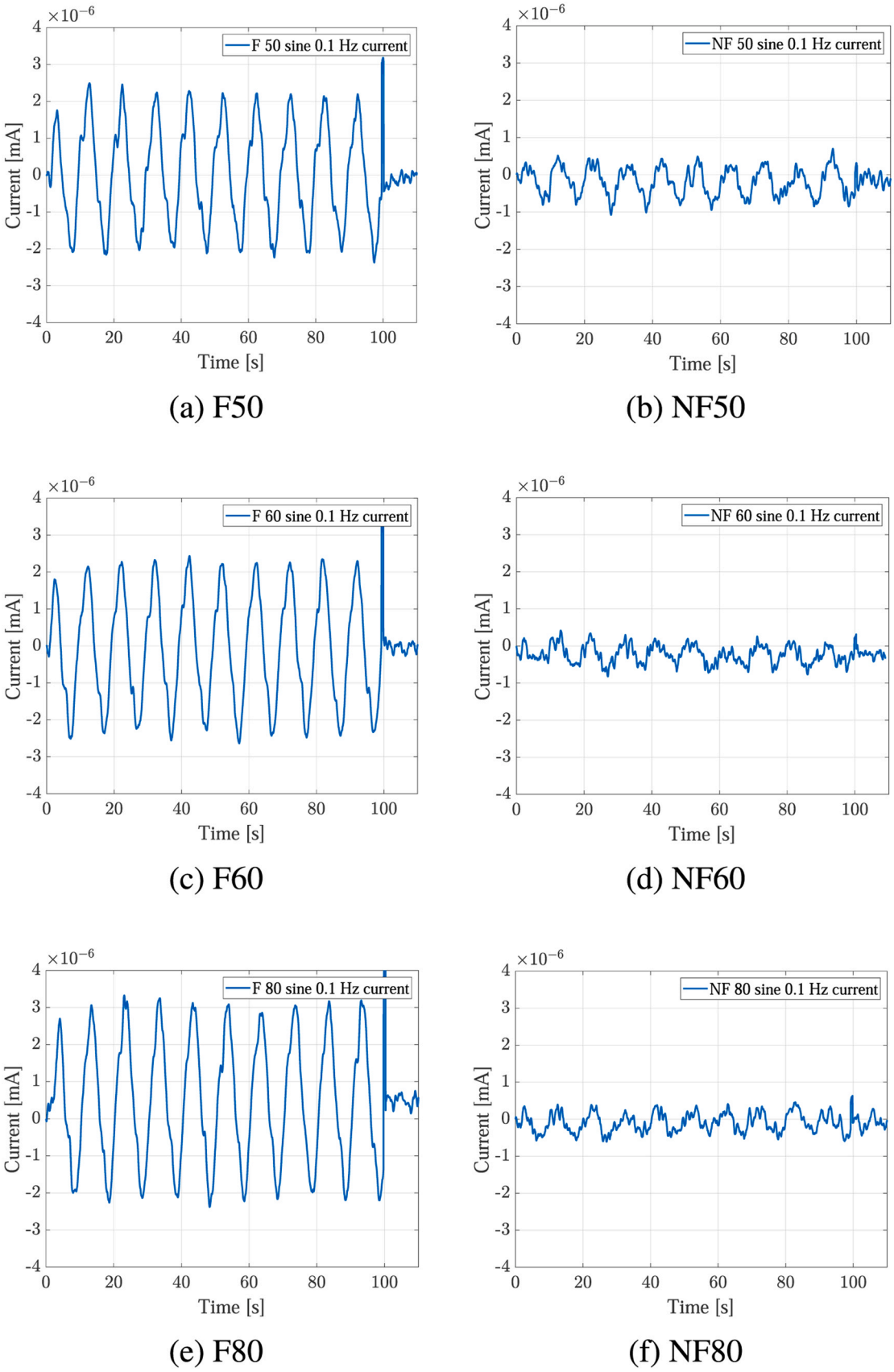


**Fig. 17.** Current flowing in the P(VDF-TrFE-CTFE)-based actuators when stimulated by a sinusoidal electric field at 0.1 Hz.

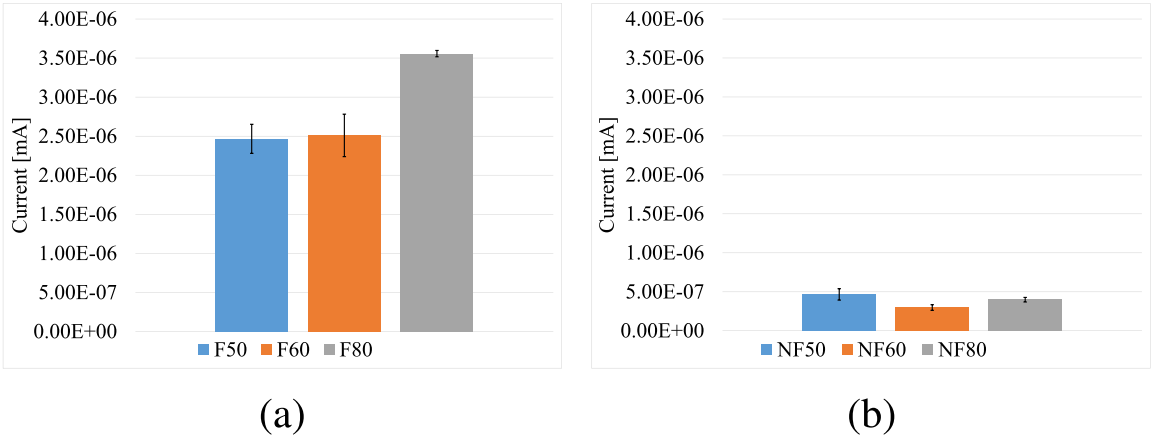


**Fig. 18.** Peak current values (mean and standard error) for (a) film-based actuators and (b) nanofibers-based actuators.

**Table 9**
Instantaneous power consumption (mW) and average power consumption (mW) of the P(VDF-TrFE-CTFE)-based actuators, when stimulated by a sinusoidal electric field of 15 MV/m at 0.1 Hz.

| Actuator | Instantaneous power [mW] | Average power [mW] |
|---|---|---|
| F50 | 1.88 | 0.649 |
| F60 | 2.22 | 0.575 |
| F80 | 4.27 | 2.033 |
| NF50 | 0.349 | 0.119 |
| NF60 | 0.267 | 0.063 |
| NF80 | 0.480 | 0.080 |

## 7. Conclusion

This study analyzes the electrostrictive effect of the P(VDF-TrFE-CTFE), in the form of both extruded film and aligned electrospun nanofiber mats, when used as active layer in unimorph cantilever beam soft actuators. The specific stiffness and the specific work of the actuators are evaluated when stimulated by a DC electric field, showing higher values in the case of the electrospun nanofibers-based actuators. Moreover, the blocking forces and the tip deflections of the actuators, when stimulated by a AC electric field, are also evaluated, showing a faster viscoelastic relaxation in the case of the electrospun nanofibers-based actuators. Finally, the current flowing in the actuators, when stimulated by an AC electric field, is evaluated, demonstrating a lower electrical power consumption in the case of nanofibers-based actuators. This study concludes that the electrospun aligned P(VDF-TrFE-CTFE) nanofibers have a high potential in the field of electrostrictive actuators, due to their high specific properties, fast viscoelastic relaxation, and low electrical power consumption.

## CRediT authorship contribution statement

**Riccardo D'Anniballe:** Methodology, Formal analysis, Investigation, Data curation, Writing – original draft, Visualization. **Andrea Zucchelli:** Conceptualization, Formal analysis, Writing – review & editing, Supervision. **Raffaella Carloni:** Conceptualization, Formal analysis, Writing – review & editing, Supervision, Project administration, Funding acquisition.

## Declaration of Competing Interest

The authors declare that they have no known competing financial interests or personal relationships that could have appeared to influence the work reported in this paper.

## Acknowledgments

This work was funded by the European Commission's Horizon 2020 Programme as part of the project MAGNIFY under grant no. 801378.

The authors would like to thank Dr. Alessio Marrani (Solvay Specialty Polymers, Italy) for the production of the films of P(VDF-TrFE-CTFE), and Giacomo Selleri (doctoral candidate in the Department of Electrical, Electronic and Information Engineering "Guglielmo Marconi", University of Bologna, Italy) for providing the SEM images of the P(VDF-TrFE-CTFE) electrospun nanofiber mats.

## References

[1] H. Xu, Z. Cheng, D. Olson, T. Mai, Q.M. Zhang, Ferroelectric and electromechanical properties of poly(vinylidene-fluoride-trifluoroethylene-chlorotrifluoroethylene) terpolymer, Appl. Phys. Lett. 78 (16) (2001) 2360–2362.
[2] Z. Yu, C. Ang, L.E. Cross, A. Petchsuk, T.C. Chung, Dielectric and electroactive strain properties of poly(vinylidene-fluoride-trifluoroethylene-chlorotrifluoroethylene) terpolymers, Appl. Phys. Lett. 84 (10) (2004) 1737–1739.
[3] R. O'Connor, G. McGuinness, Electrospun nanofibre bundles and yarns for tissue engineering applications: a review, Proc. Inst. Mech. Eng. Part H J. Eng. Med. 230 (11) (2016) 987–998.
[4] J.-M. Park, G.-Y. Gu, Z.-J. Wang, D.-J. Kwon, P. Shin, J.-Y. Choi, K.L. DeVries, Mechanical and electrical properties of electrospun cnt/pvdf nanofiber for micro-actuator applications, Adv. Compos. Mater. 25 (4) (2016) 305–316.
[5] N. Tohluebaji, H. Putson, N. Muensit, High electromechanical deformation based on structural beta-phase content and electrostrictive properties of electrospun poly(vinylidene fluoride- hexafluoropropylene) nanofibers, Polymers 11 (11) (2019).
[6] J. Pu, X. Yan, Y. Jiang, C. Chang, L. Lin, Piezoelectric actuation of direct-write electrospun fibers, Sens. Actuators A Phys. 164 (1–2) (2010) 131–136.
[7] H. Imamura, K. Kadooka, M. Taya, A variable stiffness dielectric elastomer actuator based on electrostatic chucking, Soft Matter 13 (18) (2017) 3440–3448.
[8] Q. Liu, C. Richard, J.F. Capsal, Control of crystal morphology and its effect on electromechanical performances of electrostrictive p(vdf-trfe-ctfe) terpolymer, Eur. Polym. J. 91 (2017) 46–60.
[9] N.D.K. Tu, M.-S. Noh, Y. Ko, J.-H. Kim, C.Y. Kang, H. Kim, Enhanced electromechanical performance of p(vdf-trfe-ctfe) thin films hybridized with highly dispersed carbon blacks, Compos. Part B Eng. 152 (2018) 133–138.

[10] R. Carloni, V.I. Lapp, A. Cremonese, J. Belcari, A. Zucchelli, A variable stiffness joint with electrospun P(VDF-TrFE-CTFE) variable stiffness springs, IEEE Robot. Autom. Lett. 3 (2) (2018) 973–978.
[11] R. D'Anniballe, A. Zucchelli, R. Carloni, Towards poly(vinylidene fluoride-trifluoroethylene-chlorotrifluoroethylene)-based soft actuators: films and electrospun aligned nanofiber mats, Nanomaterials 11 (1) (2021).
[12] N. Bhardwaj, S.C. Kundu, Electrospinning: a fascinating fiber fabrication technique, Biotechnol. Adv. 28 (3) (2010) 325–347.
[13] B. Qiao, X. Wang, S. Tan, W. Zhu, Z. Zhang, Synergistic effects of Maxwell stress and electrostriction in electromechanical properties of poly(vinylidene fluoride)-based ferroelectric polymers, Macromolecules 52 (22) (2019) 9000–9011.
[14] K. Ikushima, S. John, K. Yokoyama, S. Nagamitsu, A practical multilayered conducting polymer actuator with scalable work output, Smart Mater. Struct. 18 (9) (2009) 095022.
[15] S. Wang, Q. Li, Design, synthesis and processing of PVDF-based dielectric polymers, IET Nanodielectr. 1 (2) (2018) 80–91.
[16] W. Liu, S. Thomopoulos, Y. Xia, Electrospun nanofibers for regenerative medicine, Adv. Healthc. Mater. 1 (1) (2012) 10–25.
[17] B. Zaarour, L. Zhu, C. Huang, X. Jin, H. Alghafari, J. Fang, T. Lin, A review on piezoelectric fibers and nanowires for energy harvesting, J. Ind. Text. 51 (2) (2021) 297–340.
[18] R. D'Anniballe, G. Paoletta, R. Carloni, A polyurethane-based electrospun nanofiber bundle soft actuator: fabrication, modeling, and control, IEEE Int. Conf. Soft Robot. (2021) 393–398.
[19] C. Gotti, A. Sensini, A. Zucchelli, R. Carloni, M.L. Focarete, Hierarchical fibrous structures for muscle-inspired soft-actuators: a review, Appl. Mater. Today 20 (2020) 100772.
[20] S.B. Kang, S.H. Won, M.J. Im, C.U. Kim, W.I. Park, J.M. Baik, K.J. Choi, Enhanced piezoresponse of highly aligned electrospun poly (vinylidene fluoride) nanofibers, Nanotechnology 28 (39) (2017) 395402.
[21] P. Katta, M. Alessandro, R. Ramsier, G. Chase, Continuous electrospinning of aligned polymer nanofibers onto a wire drum collector, Nano Lett. 4 (11) (2004) 2215–2218.
[22] H. Pan, L. Li, L. Hu, X. Cui, Continuous aligned polymer fibers produced by a modified electrospinning method, Polymer 47 (14) (2006) 4901–4904.
[23] B. Zaarour, L. Zhu, C. Huang, X. Jin, Enhanced piezoelectric properties of randomly oriented and aligned electrospun pvdf fibers by regulating the surface morphology, J. Appl. Polym. Sci. 136 (6) (2019) 47049.
[24] D. Fabiani, F. Grolli, G. Selleri, M. Speranza, T. Brugo, E. Maccaferri, D. Cocchi, A. Zucchelli, Nanofibrous piezoelectric structures for composite materials to be used in electrical and electronic components, Proc. Nord. Insul. Symp. (26) (2019) 1–5.
[25] T. Sharma, S. Naik, J. Langevine, B. Gill, J.X. Zhang, Aligned pvdf-trfe nanofibers with high-density pvdf nanofibers and pvdf core-shell structures for endovascular pressure sensing, IEEE Trans. Biomed. Eng. 62 (1) (2014) 188–195.
[26] A. Dodero, E. Brunengo, M. Castellano, S. Vicini, Investigation of the mechanical and dynamic-mechanical properties of electrospun polyvinylpyrrolidone membranes: a design of experiment approach, Polymers 12 (7) (2020) 1524.
[27] A. Sensini, C. Gualandi, L. Cristofolini, G. Tozzi, M. Dicarlo, G. Teti, M. Mattioli-Belmonte, M.L. Focarete, Biofabrication of bundles of poly (lactic acid)-collagen blends mimicking the fascicles of the human achille tendon, Biofabrication 9 (1) (2017) 015025.
[28] M. Sitti, D. Campolo, J. Yan, R.S. Fearing, Development of PZT and PZN-PT based unimorph actuators for micromechanical flapping mechanisms, IEEE Int. Conf. Robot. Autom. (2001) 3839–3846.
[29] E. Maccaferri, L. Mazzocchetti, T. Benelli, A. Zucchelli, L. Giorgini, Morphology, thermal, mechanical properties and ageing of nylon 6,6/ graphene nanofibers as Nano$^2$ materials, Compos. Part B Eng. 166 (2019) 120–129.
[30] K. Prabakaran, S. Mohanty, S.K. Nayak, Improved electrochemical and photovoltaic performance of dye sensitized solar cells based on peo/pvdf-hfp/silane modified tio 2 electrolytes and mwcnt/nafion® counter electrode, RSC Adv. 5 (51) (2015) 40491–40504.
[31] B. Isaac, R.M. Taylor, K. Reifsnider, Anisotropic characterizations of electrospun pan nanofiber mats using design of experiments, Nanomaterials 10 (11) (2020).
[32] S. Ahmed, Z. Ounaies, E.A.F. Arrojado, Electric field-induced bending and folding of polymer sheets, Sens. Actuators A Phys. 260 (2017) 68–80.
[33] Q.-M. Wang, L.L. Eric Cross, Tip deflection and blocking force of soft pzt-based cantilever rainbow actuators, J. Am. Ceram. Soc. 82 (1) (1999) 103–110.
[34] M.K. Yongjun Lai, James McDonald, T. Hubbard, Force, deflection and power measurements of toggled microthermal actuators, J. Micromech. Microeng. 14 (2003) 49.
[35] E. Acome, S.K. Mitchell, T.G. Morrissey, M.B. Emmett, C. Benjamin, M. King, M. Radakovitz, C. Keplinger, Hydraulically amplified self-healing electrostatic actuators with muscle-like performance, Science 359 (6371) (2018) 61–65.
[36] C.C. Foo, S. Cai, S.J.A. Koh, S. Bauer, Z. Suo, Model of dissipative dielectric elastomers, J. Appl. Phys. 111 (3) (2012) 034102.
[37] J. Zou, G. Gu, Modeling the viscoelastic hysteresis of dielectric elastomer actuators with a modified rate-dependent prandtl-ishlinskii model, Polymers 10 (5) (2018).
[38] K. Kadooka, H. Imamura, M. Taya, Experimentally verified model of viscoelastic behavior of multilayer unimorph dielectric elastomer actuators, Smart Mater. Struct. 25 (10) (2016) 105028.
[39] L. Liu, H. Chen, J. Sheng, J. Zhang, Y. Wang, S. Jia2, Experimental study on the dynamic response of in-plane deformation of dielectric elastomer under alternating electric load, Smart Mater. Struct. 10 (5) (2014) 025037.
[40] D.Q. Tran, J. Li, F. Xuan, T. Xiao, Viscoelastic effects on the actuation performance of a dielectric elastomer actuator under different equal, un-equal biaxial prestretches, Mater. Res. Express 5 (6) (2018) 065303.
[41] F. Pedroli, A. Marrani, M.-Q. Le, O. Sansau, P.-J. Cottinet, J.-F. Capsal, Reducing leakage current and dielectric losses of electroactive polymers through electro-annealing for high-voltage actuation, RSC Adv. 9 (23) (2019) 12823–12835.
[42] S. Hammami, A. Sylvestre, F. Jomni, C. Jean-Mistral, Electrical conduction in dielectric elastomer transducers, IEEE Trans. Dielectr. Electr. Insul. 27 (1) (2020) 17–25.

**Riccardo D'Anniballe:** received the BSc and MSc degree in energy engineering from the University of Bologna, Italy, in 2015 and 2018, respectively. He is currently a doctoral candidate in the Bernoulli Institute for Mathematics, Computer Science, and Artificial Intelligence, Faculty of Science and Engineering, University of Groningen. His research interests include design, modeling, and control of novel (soft) actuators.

**Andrea Zucchelli:** received the MSc degree in nuclear engineering from the University of Bologna, Italy, and the PhD degree from the Department of Industrial Engineering of the University of Bologna. From 2002 to 2017 he was Assistant Professor in Machine Design at the Department of Industrial Engineering of the University of Bologna where is an Associate Professor, since 2018. His research interests include innovative mechanical and mechatronic solutions for the production of nanofibres by electrospinning technology, development of novel nanostructured composite materials and vitreous coatings and their experimental characterization, kineto-elasto-dynamic simulation of complex mechanical systems for mechatronic applications .

**Raffaella Carloni:** received the MSc degree in electronic engineering from the University of Bologna, Italy, and the PhD degree from the Department of Electronics, Computer Science and Systems, University of Bologna. She was Assistant/Associate Professor at the University of Twente, Enschede, The Netherlands, from 2008 to 2017. She joined the University of Groningen, The Netherlands, in 2017. She is currently Associate Professor in the Bernoulli Institute for Mathematics, Computer Science, and Artificial Intelligence, Faculty of Science and Engineering, University of Groningen. Her research interests include design, modeling and control of compliant robotic systems, novel (soft) actuators, and prosthetic devices.